Supporting Information

Bagnéris et al. 10.1073/pnas.1406855111

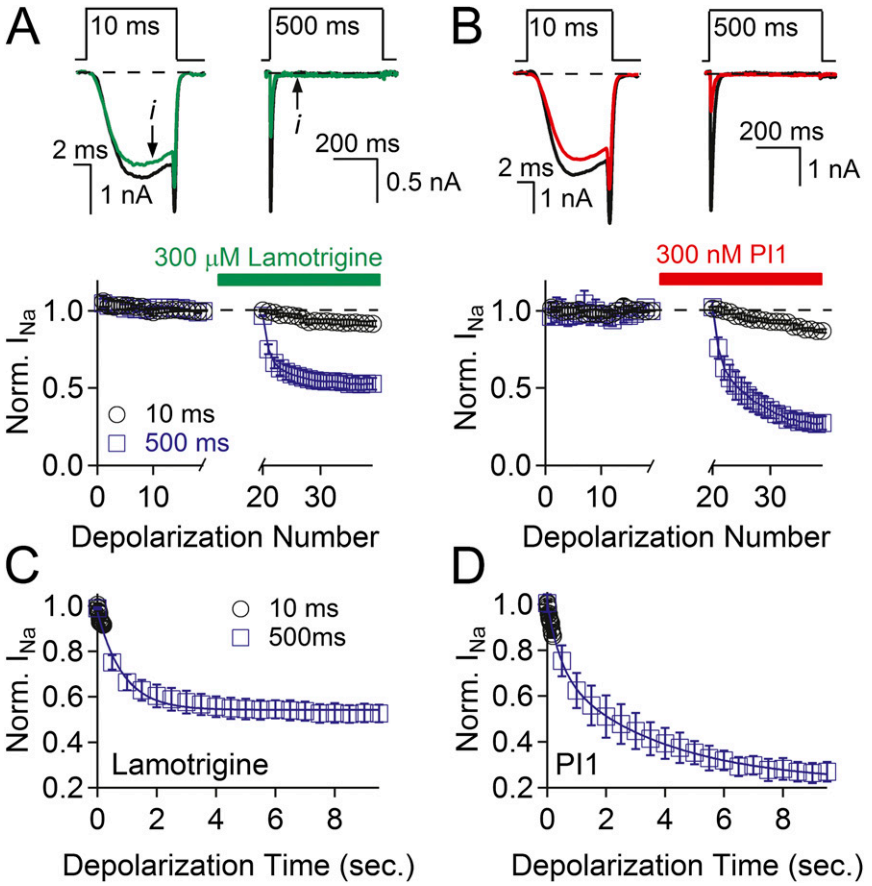

Fig. S1. Lamotrigine and PI1 preferentially bind to the open/inactivated state of the sodium channel from *Magnetococcus marinus* (NavMs). (*A* and *B*, *Upper*) Voltage-dependent Na^+ currents from transfection of cells with the NavMs construct, evoked by depolarizations for 10 ms or 500 ms to −20 mV from −180 mV holding potentials at 0.2 Hz. NavMs channels inactivate after depolarization; longer depolarization times (500 ms vs. 10 ms) increase the number of channels in the inactivated state (indicated by *i*). Black traces were measured from the last depolarization in control conditions (pulse 19). Red current traces are from the last depolarization in the presence of drug (pulse 39). (*Lower*) Resulting current magnitudes were normalized to the last pulse in control conditions (dotted line). After 2 min, patched clamped cells were held at −180 mV and placed in a stream of the compound indicated for 45 s (colored bar). Cells were then depolarized to assess state-dependent antagonism of the Na^+ current. (*C* and *D*) Rates of current block based on depolarization time. Because NavMs inactivates as a function of depolarization, decays of current magnitudes were fit to a single (*C*, for lamotrigine) or double exponential (*D*, for PI1) to assess the rate of onset of current block. τ = 450 ms for lamotrigine and τ_1 = 490 ms and τ_2 = 3.7 s for PI1 (±SEM, n = 5 cells).

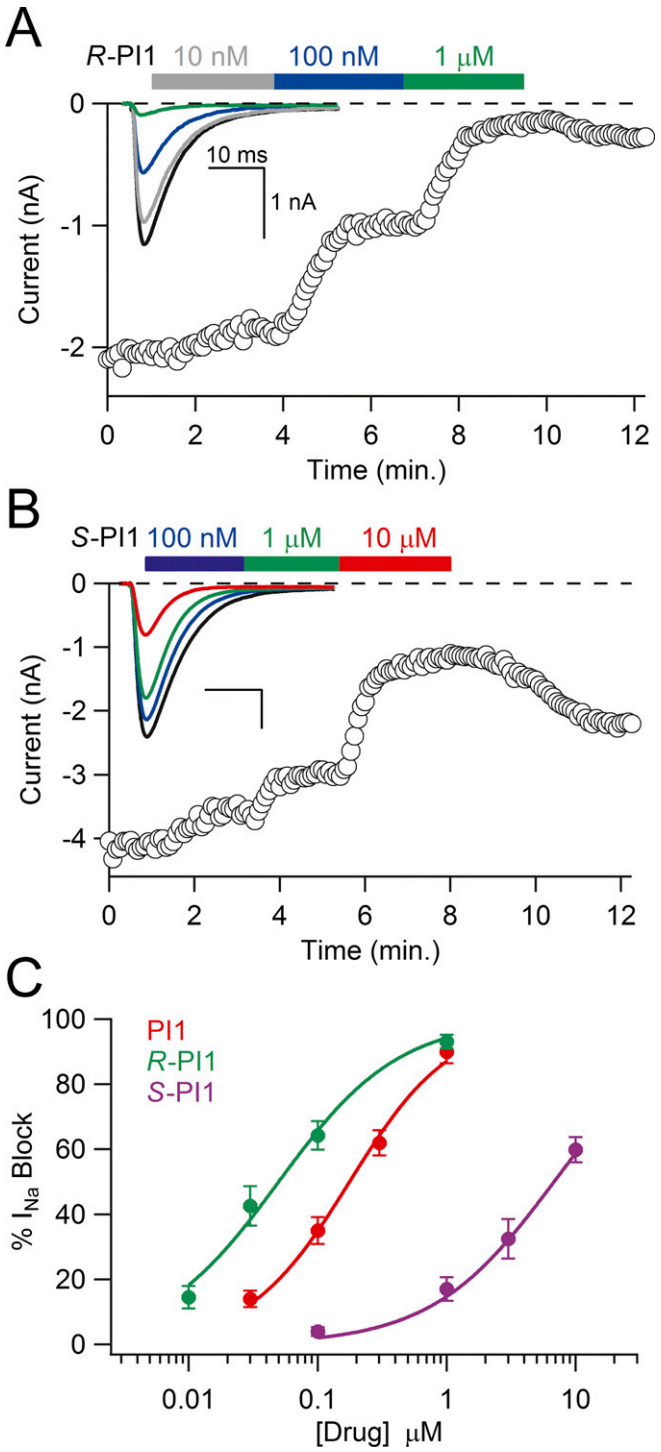

Fig. S2. The *R*- enantiomer of PI1 is a more potent sodium channel antagonist than the *S*- enantiomer. (*A* and *B*) The time course of sodium current antagonism by *R*- and *S*- PI1 enantiomers. HEK-293T cells transfected NavMs were patch clamped in the whole-cell configuration. (*Insets*) Voltage-gated Na^+ currents activated by a 0.2-Hz train of 0.5-s depolarizations to −30 from −180 mV. The onset of block was assessed after 2–3 min of extracellular application of PI1 concentrations as indicted by the colored boxes. (*C*) Concentration–I_{Na} block relationships (±SEM, n = 4–6 cells) for *R*- and *S*- enantiomers of PI1 for NavMs channels. The IC_{50} was estimated by fitting the average percent current block to the Hill equation. The IC_{50} values for *R*-PI1 and *S*-PI1 were 50 nM and 6.8 μM, respectively.

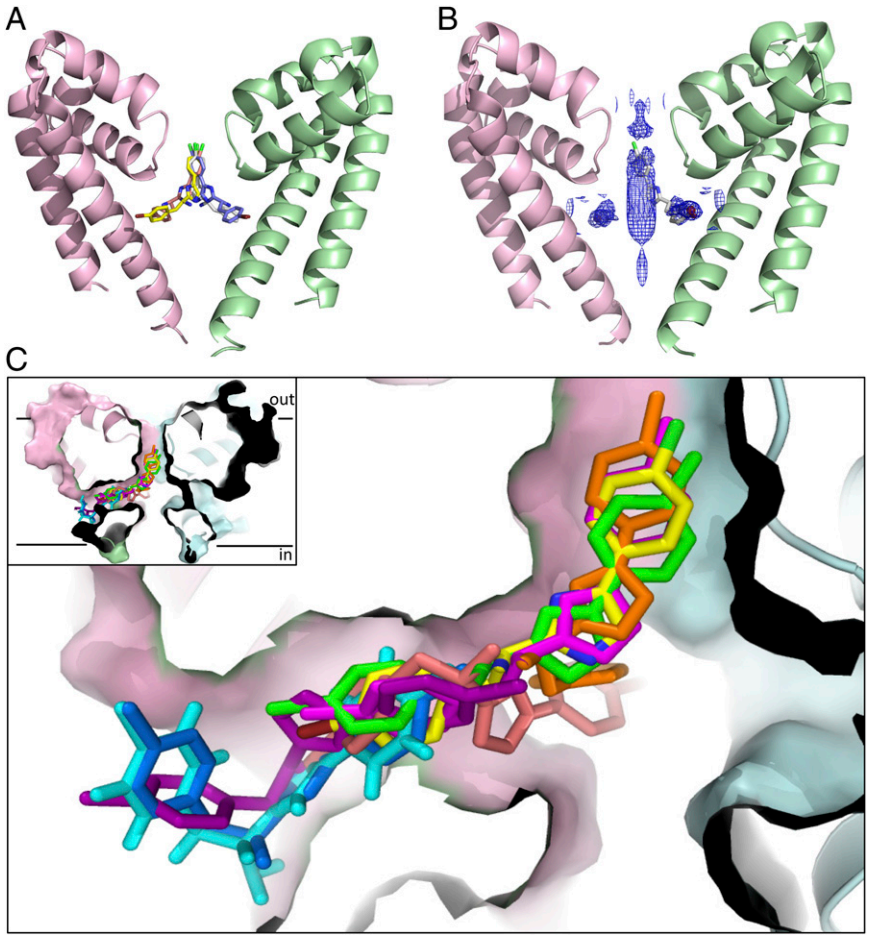

Fig. S3. Docking of the PI1 compound. (*A*) Side view showing the potential overlap of the distal ends of PI1 in the selectivity filter (SF) when it is docked into each of the four monomers. This steric clash would account for why the occupancy at any one of the sites is only ~1/4. For clarity, only two of the four polypeptide chains are shown. (*B*) Side view of the 2Fo-Fc electron density map of the PI1-containing structure contoured at a low level (0.75 σ) in the region of the selectivity filter, indicating the presence of density that could be attributable to the distal end of the compound. However, because of the four possible partially occupied positions (as in *A*) and the low density, details of its molecular structure cannot be discerned. One copy of the compound (right side of the SF) is placed in the docked position for reference. (*C*) PI1 blocker pathway to the binding site. The 10 best hits of the *R*- enantiomer from in silico docking studies on the NavMs-pore crystal structure (in surface representation) have been superposed. The fenestrations are to the left in the pink monomer, and the SF is at the upper interface between the pink and cyan monomers. This indicates a possible pathway from the membrane bilayer to the highest hit (yellow sticks, defined as the binding site) located at the top of the channel cavity. The upper left *Inset* shows where this region is in the side view of a slice through the center of the pore (same direction as in Fig. 2*F*).

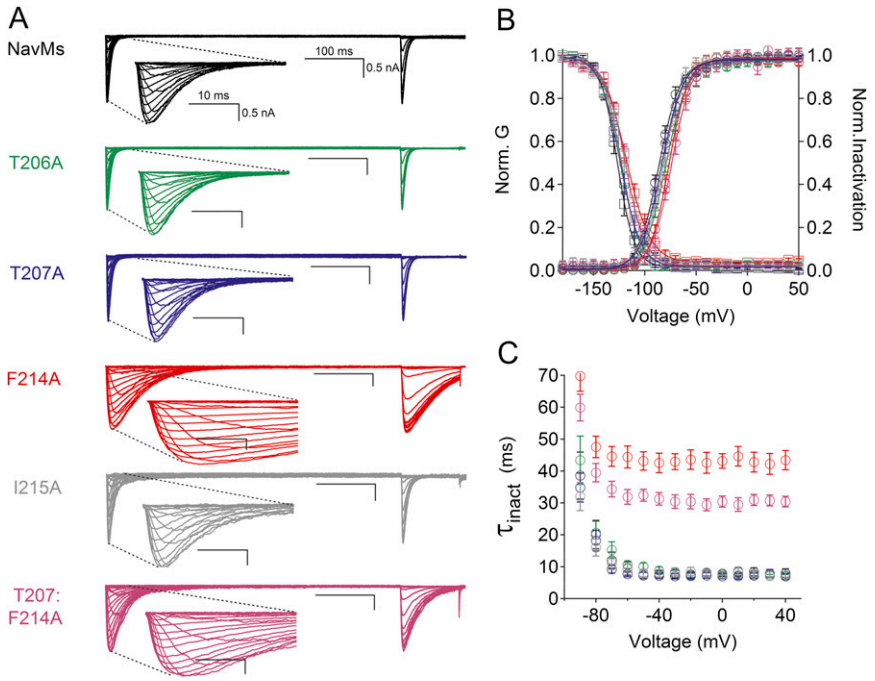

Fig. S4. Electrophysiological characterizations of mutant NavMs channels. (*A*) Example traces from HEK293T cells expressing wild-type and the mutant NavMs channels used in this study, in the absence of blocker compounds. Currents were activated by prepulses of increasing potentials at 500 ms followed by a test pulse to activated $V_{1/2} + 20$ mV. (*B*) Conductance–voltage and inactivation–voltage relationships were measured by plotting the average prepulse peak current converted to conductance and reduction of test pulse peak current as a function of prepulse potential (±SEM, $n = 5–9$) and fit to a sigmoid equation. (*C*) Voltage-inactivation rate relationship was measured by fitting the decay of current during the prepulse to a single exponential. The average rate of inactivation was plotted as a function of prepulse potential (±SEM, $n = 5–9$). The color coding for each of the mutants in *B* and *C* is as in the traces in *A*.

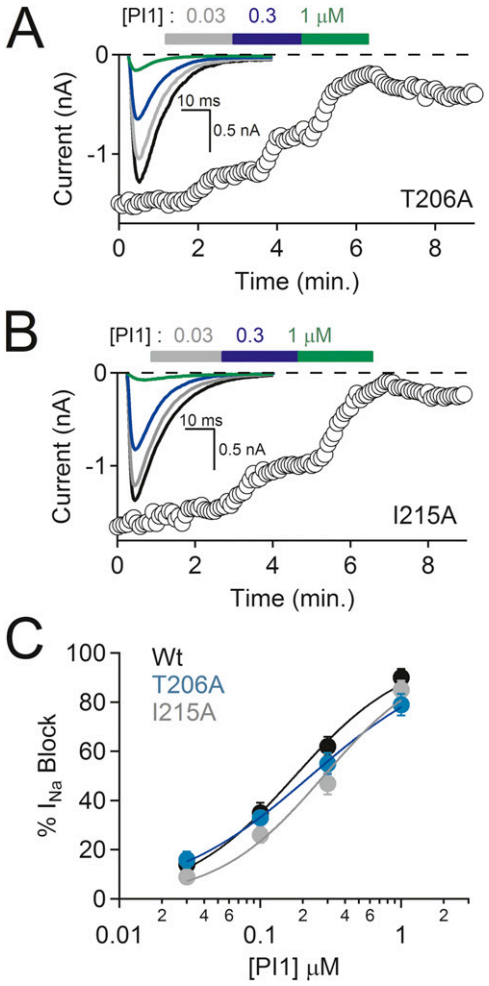

Fig. S5. Lack of effects of mutations T206A and I215A on PI1 potency. (*A* and *B*) Experiments conducted as in Figs. 1*B* and 3*B*, showing the onset of sodium current block by PI1 in HEK293T cells expressing T206A and I215A mutant NavMs channels. (*Insets*) NavMs currents activated by a 0.2-Hz train of 0.5-s depolarizations to −30 from −180 mV. (*C*) The PI1 concentration–I_{Na} block relationships for mutants T206A and I215A. The data show the lack of change in the IC_{50} potency of PI1due to the T206 and I215A mutants compared with wild-type (Wt) channels (±SEM, n = 4–6 cells). This is in contrast to the effects of the T207A and F214A mutants seen in Fig. 3*C*.

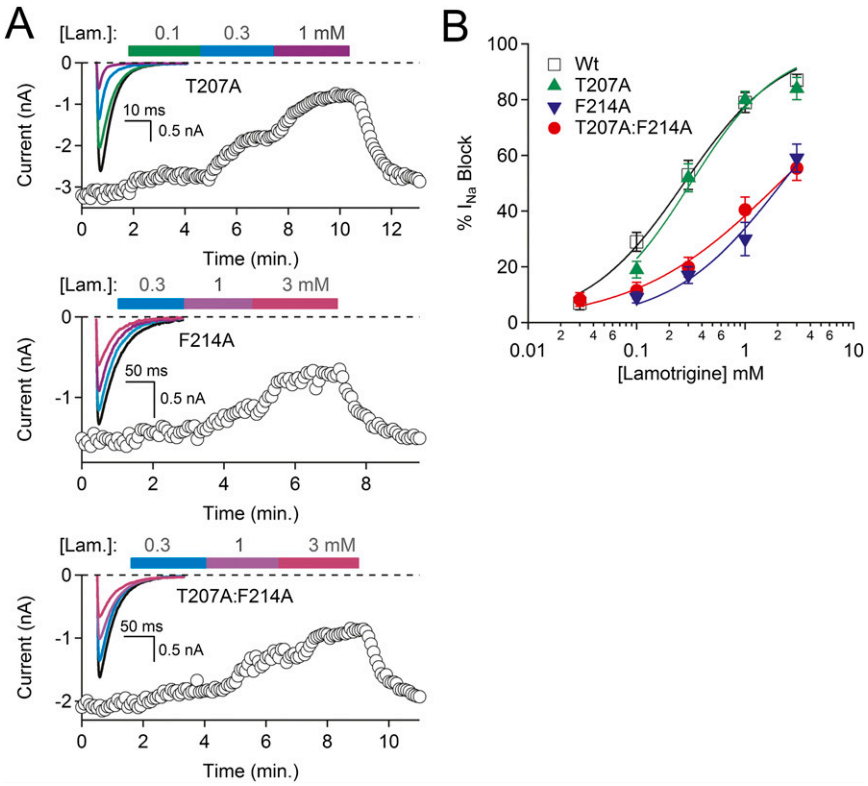

Fig. S6. Effects of mutations on lamotrigine efficacy. (*A*) Experiments showing the onset of sodium current block, conducted as in Fig. 3*A*, except using lamotrigine with the T207A, F214A, and T207A:F214A mutants. (*Insets*) NavMs currents activated by a 0.2-Hz train of 0.5-s depolarizations to −30 from −180 mV. (*B*) The lamotrigine concentration–I_{Na} block relationships showing that the potency of lamotrigine is decreased in the presence of the F214A and T207A:F214A mutations, whereas little to no change was observed for the single T207A mutant (±SEM, n = 4–5 cells).

Table S1. Data collection and refinement statistics (molecular replacement) for additional cocrystals of the NavMs pore

Parameter	PI2 complex	P13 complex	PI4 complex	PI5 complex	PI6 complex	PI7 complex
Protein Data Bank ID	4OXS	4PA3	4PA4	4P9P	4PA6	4PA7
Data collection						
Space group	$C222_1$	$C222_1$	$C222_1$	$C222_1$	$C222_1$	$C222_1$
Cell dimensions						
a, *b*, *c* (Å)	79.89, 329.02, 79.50	80.03, 331.95, 80.20	79.89, 327.33, 79.94	80.17, 330.94, 79.98	79.93, 324.57, 79.67	79.81, 328.86, 79.92
α, β, γ (°)	90.0, 90.0, 90.0	90.0, 90.0, 90.0	90.0, 90.0, 90.0	90.0, 90.0, 90.0	90.0, 90.0, 90.0	90.0, 90.0, 90.0
Resolution (Å)	45.22–2.80 (2.95–2.80)	45.5–3.24 (3.51–3.25)	45.06–3.02 (3.20–3.02)	45.41–2.91 (3.09–2.91)	44.77–3.36	45.2–3.02 (3.21–3.02)
R_{pim}	0.052 (0.22)	0.071 (0.248)	0.052 (0.231)	0.051 (0.197)	0.053 (0.176)	0.06 (0.206)
I/σI	10.6 (3.3)	8.4 (3.1)	10.8 (3.1)	12.8 (3.7)	12.0 (4.4)	9.7 (3.4)
Completeness (%)	100.0 (100.0)	98.8 (94.3)	99.6 (98.0)	98.7 (92.5)	99.7 (98.9)	99.8 (99.0)
Redundancy	8.6 (8.6)	9.5 (9.4)	9.8 (9.7)	9.9 (9.3)	13.1 (13.3)	8.7 (8.7)
Refinement						
Resolution (Å)	45.2–2.80 (2.91–2.80)	45.5–3.25 (3.45–3.25)	45.06–3.02 (3.17–3.02)	45.4–2.9 (3.04–2.9)	44.77–3.36 (3.59–3.36)	45.2–3.02 (3.17–3.02)
No. reflections	26,515 (2,945)	17,115 (2,531)	21,127 (2,752)	23,535 (2,486)	15,245 (2,654)	21,096 (2,665)
R_{work}/R_{free}	26.6/28.5 (23.4/24.3)	21.4/23.0 (21.2/22.3)	23.0/24.4 (22.4/25.0)	16.4/19.7 (18.3/25.6)	30.2/34.2 (21.7/25.8)	25.1/26.5 (22.7/23.9)
No. atoms						
Protein	2,809	2,835	2,895	2,803	2,856	2,849
Ligand/ion	251	146	107	125	80	135
Water	173	21	13	273	18	28
B-factors						
Protein	63.2	60.8	91.1	61.9	72.4	74.1
Ligand/ion	65.5	80.6	100.4	70.2	92.8	75.2
Water	47.9	38.0	53.8	65.8	24.9	36.7
rmsd						
Bond lengths (Å)	0.01	0.01	0.01	0.01	0.01	0.01
Bond angles (Å)	1.08	1.12	1.09	1.09	1.10	1.10